Available online at www.sciencedirect.com

ScienceDirect

Materials Today: Proceedings 7 (2019) 353–361

materialstoday: PROCEEDINGS

www.materialstoday.com/proceedings

BioM&M_2018

Geometric assessment of lattice materials built via Selective Laser Melting

M. Dallago[a,*], S. Raghavendra[a], V. Luchin[b], G. Zappini[b], D. Pasini[c], M. Benedetti[a]

[a]*Department of Industrial Engineering, University of Trento, Trento, Italy*
[b]*Eurocoating Spa, Pergine Valsugana, Trento, Italy*
[c]*Department of Mechanical Engineering, McGill University, Montreal, Quebec, Canada*

Abstract

Selective Laser Melting (SLM) is a technology that allows for the realization of metallic porous solids that cannot be produced with other methods. Nevertheless, a geometric discrepancy between the as-designed and as-built part is a well-known issue that can be critically important for biomedical metallic lattices with pore size and strut thicknesses of a few hundred microns. In practice, any geometric imperfection introduces a degree of uncertainty that can alter the mechanical properties of the as-built lattice. A quantitative relationship between the as-designed geometry and the real geometry is a very useful design tool because it makes possible to predict the final morphology of the lattice by considering the manufacturing errors: a more predictable geometry of the lattice structure means more predictable mechanical properties of the implant.

In this work, we investigate the relationship between the as-designed strut thickness and the printed strut thickness for regular cubic cell lattices. The joints between the struts are filleted to reduce the stress concentration and increase fatigue resistance. The size of the unit cell is scaled to find the smallest radius which can be accurately reproduced. Moreover, we also studied the effect of the printing direction on geometrical accuracy.

Selection and Peer-review under responsibility of 1st International Conference on Materials, Mimicking, Manufacturing from and for Bio Application (BioM&M).

Keywords: Cellular materials; Error compensation; Selective Laser Melting

* Corresponding author: Tel.: +39- 0461 282500; fax: +39-0461-281977
E-mail address: michele.dallago@unitn.it (M.Dallago)

1. Introduction

Selective Laser Melting (SLM) is a manufacturing method to produce metallic lattice materials with a controlled geometry that are suitable for biomedical implants. Nevertheless, when components with such a small-scale geometry are realized with this technology, significant morphological differences between the as-designed and the as-built geometry are observed. This geometric mismatch is a combination of systematic and random deviations from the original design and limits the predictability of the mechanical and biological properties of the implant [1-4]. Liu et al. [3] investigated the effect of geometric imperfections introduced in SLM metallic lattices on the mechanical properties. They have confirmed with the aid of Finite Element (FE) models based on the statistical distribution of these defects that the mismatch between the mechanical properties predicted with models based on the as-designed geometry and the experimental results strongly correlates with the number and severity of defects.

The as-built/as-designed morphological mismatch is related to the SLM process parameters such as the laser power, the scanning speed [5-7] and layer thickness [7]. It has been noted that all these parameters affect the melt pool size and thus define the final thickness of the strut. The difficulty in predicting the as-built shape is increased by the material shrinkage during solidification and cooling [8]. The inclination of the struts to the printing plane is also a factor to consider, as discussed in [5, 9, 10-12], because inclined struts are supported by loose powder which has lower thermal conductivity than the solid and thus a higher fraction of the powder is partially or completely melted compared to a vertical strut. Some authors [2; 10; 4] observed that there is a linear correlation between the as-built and the as-designed thickness of the struts: this suggests that it is possible to compensate this mismatch with post-production erosion treatments [10] or by modifying the input CAD [4]. The latter strategy, proposed by Bagheri et al. [4], consists in the definition of a geometrical compensation factor based on a statistical analysis of the error between the as-designed strut thickness and the value obtained in the as-built structure. This factor, which depends on the as-designed strut thickness and its inclination to the build plane, was successfully used to improve the fidelity of the as-fabricated metallic lattices.

Motivated by the desire to improve the fatigue resistance of SLM square cell cellular structures for biomedical implants, in previous works we introduced filleted junctions to decrease the stress concentrations [13, 14]. The cellular specimens were scanned with a uCT system and differences with the nominal model were measured in the thickness of the struts. It was also observed that the as-built fillets were highly irregular and sometimes even difficult to identify, and this showed the need for a deeper investigation of the correlation between the as-built and the as-designed geometry with the final aim of devising a model to compensate the geometrical mismatch. This paper presents the results of a metrological investigation of SLM regular square cell lattices with filleted junctions. We considered nine combinations of the geometric parameters of the unit cell and three orientations with respect to the printing direction. The junctions between the struts are filleted with a constant fillet radius. The aim of the work is to progress towards an understanding of the relationship between the as-designed geometry and the as-build geometry of SLM lattice materials. We also present a procedure to analyze the geometry of lattice materials by using pictures taken with an optical microscope. This approach is less accurate than that based on CT scans, but it is much less expensive and to some extent faster. The metrological characterization of the specimens was carried out with an image segmentation routine developed in MATLAB, using pictures taken with a stereo microscope. The as-built geometry was extracted and compared with the as-designed geometry. The data were analyzed statistically, and a set of mathematical relationships was obtained between the as-built and the as-designed geometric parameters.

2. Materials and methods

2.1. *Cellular specimens*

The cellular specimens studied in this work have regular square cells. The struts are circular in section with constant diameter t_0 and the joints between the struts are filleted with constant fillet radius R; the size of the unit cell is L (Figure 1). Nine combinations of the geometric parameters have been considered, as listed in Table 1. The geometry is scaled up with respect to what is normally used in biomedical implants [15] because the aim is to find

the smallest radius which can be accurately reproduced with SLM. The structures have been designed to have an elastic modulus of 3 GPa, according to the procedure described in [16].

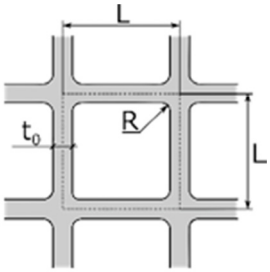

Figure 1. Regular square cell geometric parameters.

Table 1. Geometric parameters of the specimens.

# Specimen	L (μm)	t0 (μm)	R (μm)
1	4000	700	200
2	4000	680	400
3	4000	670	600
4	6000	1060	300
5	6000	1030	600
6	6000	1000	900
7	8000	1410	400
8	8000	1370	800
9	8000	1340	1200

The effect of the printing direction on the as-built geometry was investigated by printing each of the nine geometries at three orientations, as illustrated in Figure 2. In Figure 2a, one series of struts (Z) is parallel to the printing direction while the other two are perpendicular. In Figure 2b, the specimen is oriented in such a way that one series of struts (X) is perpendicular to the printing direction while the other two are inclined of 45°. In Figure 2c, the printing direction is the space diagonal of the unit cell and so all the struts are inclined of 35.26° to the printing direction. The specimens are named accordingly as "0°", "45°" and "45°-35.26°", respectively. Overall, 27 specimens were printed: nine combinations of the geometrical parameters per three printing directions.

The specimens were additively manufactured via SLM starting from the biomedical grade Ti6Al4V alloy (O_2 < 0.2%) in form of powder of diameter < 45 μm. The thickness of the discretization slices is 60 μm. A stress-relief heat treatment was applied after printing.

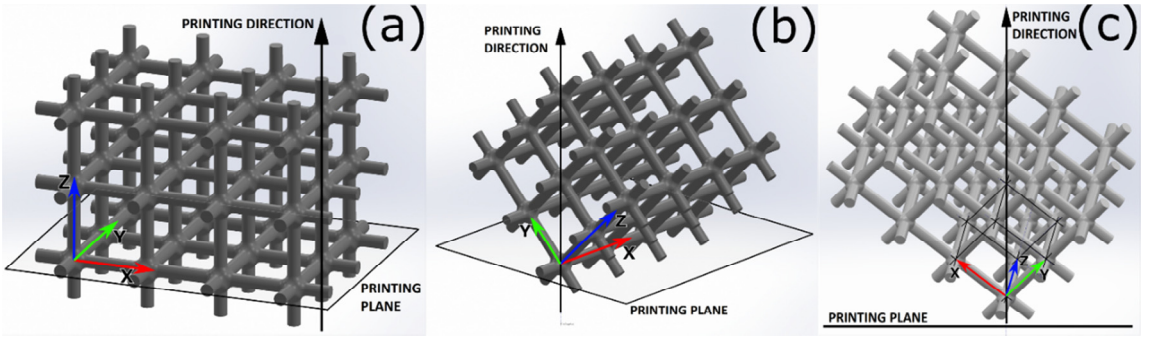

Figure 2. Orientations of the samples for printing: (a) 0°; (b) 45°; (c) 45°-35.26°.

2.2. Metrological analysis

The metrological analysis was carried out using pictures of the sides of each specimen obtained with a stereo optical microscope (Nikon SMZ25). An in-house MATLAB® routine was developed to recognize the boundaries of the specimen from the pictures using the image segmentation functions embedded in MATLAB®. The units of the acquired image are then transformed from pixels to the metric system (µm). This is schematically shown in Figure 3. The boundaries of the acquired image are the inputs for the MATLAB routine to carry out the following measurements (Figure 3b):

- Calculating the average thickness of the struts.
- Calculating the position of the center of each junction.
- Calculating the average fillet radius.
- Overlapping of the as-designed geometry to assess which parts of the unit cell are more affected by the manufacturing process.
- Calculating the distortion of the unit cell.

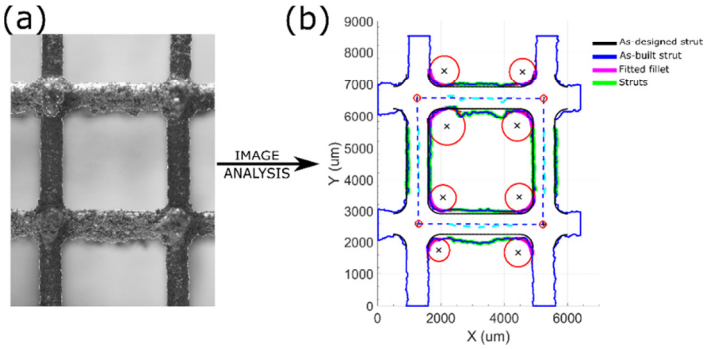

Figure 3. Example of unit cell analysis (# specimen 2, 0° orientation): (a) Recognition of the unit cell boundaries through image segmentation techniques; (b) Output of the image analysis MATLAB code that identifies and measures the main features of each picture (strut thickness, fillet radii and unit cell distortion).

The calculation of the center of the junction is the most critical part as it is the input for all the other calculations and starting from the centers of the junctions, the code is completely autonomous in recognizing the features of each picture and in carrying out the requested measurements. The advantage of this approach is that a great number of images can be quickly analyzed with minimal human intervention. Given the irregularities of the struts and the possible distortions of the unit cell, the centers of the junctions are estimated by calculating the centroid of the junction with an iterative procedure. Given a first estimation of the center from the as-designed geometry, a selection square of suitable size (the smallest possible to include the whole junction) is defined around the junction and its center is translated iteratively until the areas of the four corners are all equal inside a specified tolerance (5%), as shown in Figure 4a. At that point, the center of the square and the center of the junction coincide.

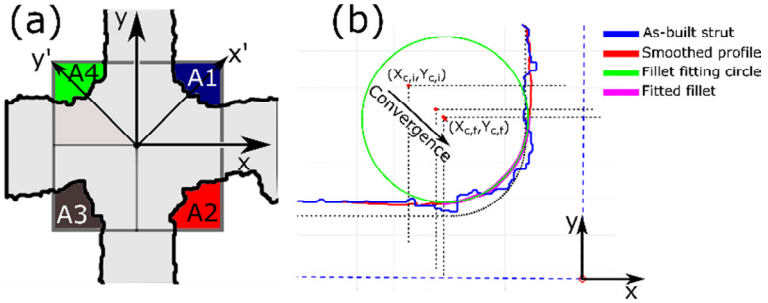

Figure 4. (a) Finding the center of the junction. (b) Measurement of the fillet radius: ($X_{c,i}$; $Y_{c,i}$) is the first guess for the center of the fillet while ($X_{c,f}$; $Y_{c,f}$) is the converged result.

The as-built fillet radius is measured by fitting the as-built profile with a circle. Estimating the fillet radius is a non-trivial task given the irregularity of the profile and often it is not clear where the fillet ends, and the strut starts. To ensure that the reasonably best fit is always found, an iterative procedure is applied. Starting from an initial guess, the points of the profile are selected and fitted with a circle. The center of the circle is used to select the new set of points to fit (indicated by the dashed lines in Figure 4b) and this procedure is continued until the center of the circle is less than a given distance (5% in our case) from the previous center. The quality of the fit is ensured by the condition that the normalized root mean square deviation (NRMSD) of the residuals is below 5%. To improve the performance of the iterative routine, the profile of the as-built radius is smoothed (MATLAB ® moving average lowpass filter) [17].

The average thickness of the struts is calculated by sampling 100 points along the strut axis and by measuring the distance normal to the axis between the profile points of the struts (Figure 5a). The as-designed geometry is overlaid on the as-built geometry by using the centers of the junction and the result can be seen in Figure 5a. The optimal overlap is found by minimizing the sum of the squares of the distances between the corresponding centers of the as-designed (asterisks in Figure 5a) and as-built geometries (red circles in Figure 5a). The precise overlay is useful to measure the distance between the as-built and as-designed profiles. This is used to measure in which parts of the specimen the ideal geometry is reproduced the worst or the best. In Figure 5b, a detail is shown of the quantitative comparison between the as-build (blue) and as-designed (black) profiles. The distances (normal to the strut axis) between the two profiles are sampled. The excess material (red) is defined positive while the lack of material (green) is defined negative.

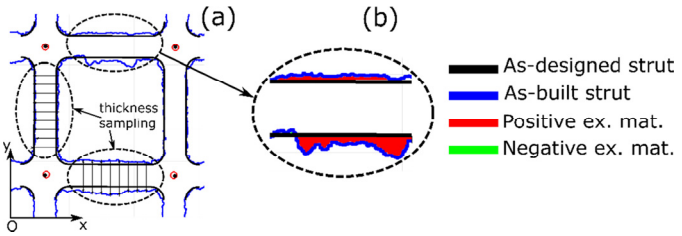

Figure 5. Superposition of the as-designed geometry on the as-built geometry and calculation of the excess material. (a) Entire unit cell; (b) Detail regarding the calculation of the excess material.

The distortion of the as-built unit cell is evaluated by calculating the error on the length of the sides and on the diagonals of the square defined by the centers of the junctions, as in Eq. 1.

$$Error(\%) = \frac{AsBuilt - AsDesigned}{AsDesigned} \times 100 \tag{1}$$

A statistical analysis was carried out on these measurements and the results are presented as mean values with the associated standard deviation. The struts of each sample type are named with respect to an *XYZ* reference system (Figure 2). For each specimen, pictures of two unit cells per each $XY - XZ - YZ$ plane were taken (Figure 6). It was not possible to obtain a picture of the whole face of a sample suitable for the segmentation procedure due to the difficulty in taking an image without shadows and with a perfect alignment of the struts to avoid including into the picture also the rows of struts below the top plane. Thus, for each specimen a total of six pictures were used to take the measurements.

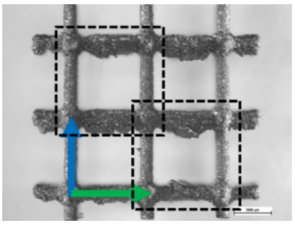

Figure 6. The dashed lines indicate how the pictures for the analysis were taken.

3. Results and discussion

The as-built strut thickness strongly depends on both the as-designed geometry and on the orientation of the strut to the printing direction (Figure 7a).

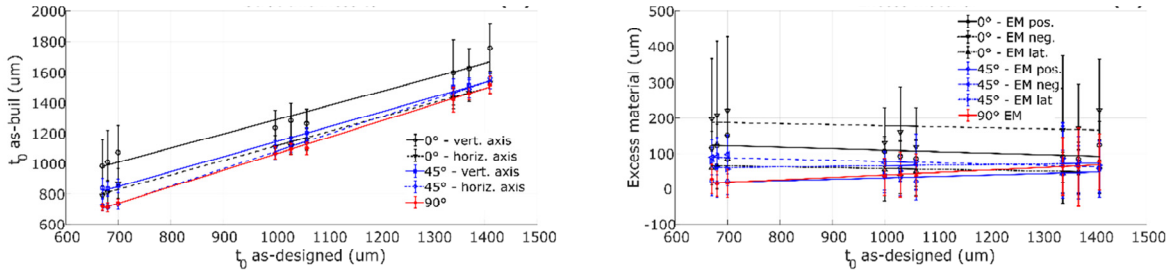

(a) (b)

Figure 7. (a) As-built strut thickness vs as-designed thickness. (b) Excess material vs as-designed thickness. The linear regression lines are plot together with the experimental data.

The results do not appear to indicate any influence of the orientation of the entire specimen (Figure 2), but it is the angle to the printing direction of the individual strut that correlates with the as-built thickness. The relationship between the as-built and the as-designed thickness is well represented by a linear function for all the orientations (0°, 45° and 90° to the printing plane), as shown in Figure 7a. The as-built thickness is always higher than the as-designed thickness and the slope of the straight lines is near to one, indicating that the quantity of material in excess is roughly constant (Figure 7b). In other words, the SLM process adds an offset to the struts that depends mainly on their orientation to the printing direction. The struts other than parallel to the printing direction have a section that can be approximated by an ellipse defined by a vertical axis that belongs to a plane normal to the printing plane and a horizontal axis normal to the printing direction, as schematically shown in Figure 8a. The vertical axis is always larger than the horizontal axis. The horizontal struts reproduce the worst the as-designed geometry because they are considerably thicker along the vertical axis of the section. It is thus advisable to avoid as much as possible to print a cellular component with struts laying in the printing plane. The as-built vertical struts on the other hand retain the circular section with a diameter close to the as-designed value.

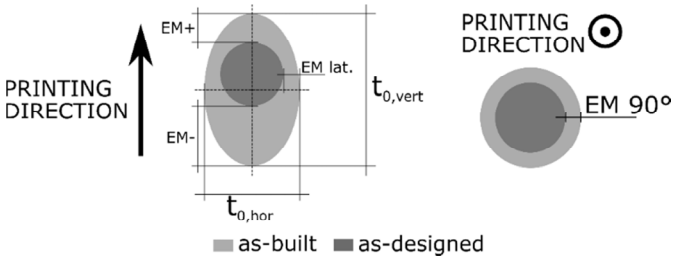

Figure 8. (a) As-built vs as-designed sections for the struts normal or inclined to the printing direction. (b) As-built vs as-designed sections for the struts aligned with the printing direction.

The plot of Figure 7a does not indicate where on the struts the material in excess accumulates: the superposition of the as-designed profile on the as-built profile is the key to obtain this information. As already introduced, the material in excess is always positive, that is, the as-built struts are on average thicker than the as-designed. The amount of excess material depends mainly on the orientation of the struts to the printing direction and to a lower degree on the as-designed thickness. The weak dependence on the thickness can be due to the higher rate at which heat is carried away by thicker struts, thus reducing the amount of melted powder. The nomenclature regarding the excess material is shown in Figure 8. The struts parallel to the printing plane (0°) show the greatest difference between the as-built and the as-designed geometries, with most of the material accumulated below the strut (as in

Figure 8a). This behavior is also observed in the inclined struts, although to a lesser extent. This is because the inclined strut is built on loose powder, which has lower thermal conductivity than the solid material. Indeed, the values of the excess material are much closer for the inclined struts than for the horizontal struts (this can be also observed in Figure 7a) and this, coupled with the wide scatter of the data, makes it harder to pick out a clear trend. The vertical struts have the lowest distance between the as-designed and the as-built profiles, which is also uniformly distributed around the section, as shown in Figure 8b.

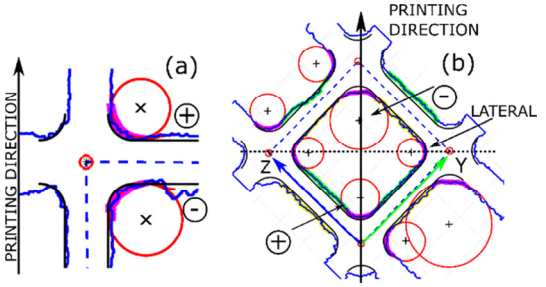

Figure 9. Classification of the fillets considering the printing direction: (a) XZ and YZ planes in the "0°" sample and XY and XZ planes in the "45°" sample; (b) YZ planes in the "45°" sample and all the planes in the "45°-35.26°" sample.

The fillet radius shows the greatest complexity in behavior as it depends both on the as-designed fillet radius and on the as-designed strut thickness. In addition, the fillet radius is strongly influenced by its orientation to the printing direction. The relationship with both as-designed geometric parameters is linear, thus the as-built fillet radius can be described by a plane. To have a meaningful representation of the data, the fillets have been classified into six categories for statistical purposes based on their location in the structure with respect to the printing direction, as shown in Figure 9. In the case of the 0° sample, the authors have distinguished between *positive fillets* (above the strut if we take the printing direction as a reference) and *negative fillets* (below the strut) for the vertical planes. This classification was applied also to the inclined planes of the 45° sample (planes XZ and XY of Figure 2b). The radii laying the horizontal plane of the 0° sample are called *horizontal fillets* (not shown in Figure 9). The fillets of the vertical planes of the 45° sample (plane YZ in Figure 2b) and of all the planes of the 45°-45° sample are classified into three categories, as shown in Figure 9b: *negative*, *positive* and *lateral*. The discussion of the results is supported only by showing the regression planes of the data for the "45°" samples due to the limited space of this article.

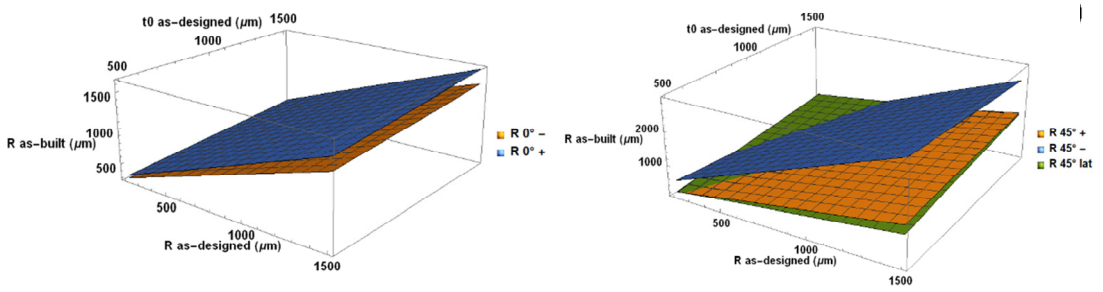

(a) (b)

Figure 10. As-built fillet radius as a function of R as-designed and t_0 as-designed for sample "45°": (a) planes XY and XZ; (b) plane YZ.

The 0° sample shows very small differences between the radii measured in the top plane (XY) and the positive radii measured in the vertical planes. The negative fillets are smaller than the other two, and this may be because a considerably thicker layer of excess material accumulates below the horizontal struts than around the vertical struts, thus "closing" the fillet (observe the profile shown in Figure 9a). The inclined planes of the 45° sample show the same behavior for the negative and positive radii as the vertical planes for the 0° sample (Figure 10a). In the vertical

planes of the 45° samples, the unit cells are tilted of 45° to the printing direction, as shown in Figure 9b. In this case, the negative fillets are considerably greater than the lateral and positive fillets (Figure 10b). The physical reason for this is that the material tends to accumulate on the negative fillets and the consequence is a "flattening" of the fillet. This is also clearly observable in Figure 9b. The planes of the 45°-45° sample are all inclined of a given angle to the printing direction. The negative fillets are consistently larger than all the other, arguably for the same reason as for the 45° sample. In general, the values of the fillet radii are very scattered and make it hard to identify a specific trend, but on the other hand the shape of the as-built fillets is regular (Figure 9) indicating that this feature can be successfully reproduced. The authors recognize that a higher number of measurements and of samples are needed to obtain more representative statistics.

The distortion of the unit cells is very low (between -0.5% and +2%) for all the geometries and all the printing directions. There appears to be no correlation between the unit cell distortion and the as-designed geometry or the printing direction.

4. Conclusions

The following conclusions can be drawn:

i. The distortion of the unit cell is minimal, even for the largest cells: it is always below 2% and positive, apart from 0° sample (small negative values).

ii. There is a linear relationship between the as-designed and the as-built strut thickness. The section of the struts inclined to an angle different from 0° to the printing direction are elongated in the printing direction.

iii. Excess material is added to the struts during the printing process due the excessive local melting and bonding of partially melted particles. The distribution of the excess material depends on the inclination to the printing direction. In general, the material tends to accumulate below the struts (with respect to the printing direction). The most affected are the horizontal struts, the least affected are the vertical struts. There is a weak dependence of the quantity of the excess material on the thickness of the struts.

iv. The as-built fillet radius depends mainly on the as-designed fillet radius, but it is also influenced by the as-designed strut thickness t_0. The fillet radius in a plane of observation depends on its orientation to the printing direction and on the thickness of both the struts that define it. The fillets that are bisected by the printing direction and face downwards (negative fillets) appear consistently larger due to the excess material.

The functions that relate the as-built geometric parameters with the as-designed parameters can be used to predict the outcome of a printing process given a specific design, provided that the process parameters are prescribed. Thus, compensation models can be developed, that can help the designer to correct the as-designed model to include the geometrical errors introduced by the production process so that the as-built shape is exactly the desired shape [4]. This work represents a first step in this direction.

References

[1] J. Parthasarathy, B. Starly, S. Ramana, A. Christensen, Journal of the Mechanical Behavior of Biomedical Materials 3 (2010), 249–259.
[2] S. Van Bael, G. Kerckhofs, M. Moesen, G. Pyka, J. Schrooten, J.P. Kruth, Materials Science and Engineering A 528 (2011), 7423–7431.
[3] L. Liu, P. Kamm, F. Garcia-Moreno, J. Banhart, D. Pasini, Journal of the Mechanics and Physics of Solids 107 (2017), 160–184.
[4] Z. S. Bagheri, D. Melancon, L. Liu, R. B. Johnston, D. Pasini, Journal of the Mechanical Behavior of Biomedical Materials 70 (2017), 17–27.
[5] L. Mullen, R. C. Stamp, W. K. Brooks, E. Jones, C. J. Sutcliffe, J Biomed Mater Res B Appl Biomater 89(2) (2009), 325–334.
[6] C. Qiu, S. Yue, N. J. E. Adkins, M. Ward, H. Hassanin, P. D. Lee, P. J. Withers, M. M. Attallah, Materials Science & Engineering A 628 (2015), 188–197.
[7] S. L. Sing, F. E. Wiria, W. Y. Yeong, Robotics and Computer–Integrated Manufacturing 49 (2018), 170–180.
[8] Z. Zhu, N. Anwer, L. Mathieu, Procedia CIRP 60 (2017), 211–216.
[9] C. Emmelmann, P. Scheinemann, M. Munsch, V. Seyda, Physics Procedia 12 (2011), 375–384.
[10] G. Pyka, G. Kerckhofs, I. Papantoniou, M. Speirs, J. Schrooten, M. Wevers, Materials 6 (2013), 4737–4757.
[11] C. Yan, L. Hao, A. Hussein, P. Young, D. Raymont, Materials and Design 55 (2014) 533–541.
[12] J. Kessler, N. Balc, A. Gebhardt, and K. Abbas, MATEC Web of Conferences 137, 02005 (2017)
[13] M. Dallago, V. Fontanari, B. Winiarski, F. Zanini, S. Carmignato, M. Benedetti, Structural Integrity Procedia 7 (2017), 116–123.

[14] M. Dallago, V. Fontanari, E. Torresani, M. Leoni, C. Pederzolli, C. Potrich, M. Benedetti, Journal of the Mechanical Behavior of Biomedical Materials 78 (2018), 381–394.
[15] N. Taniguchi, S. Fujibayashi, M. Takemoto, K. Saski, B. Otsuki, T. Nakamura, T. Matsushita, T. Kokubo, S. Matsuda, Mater. Sci. Eng. C (2016), 690–701.
[16] M. Dallago, M. Benedetti, V. Luchin, V. Fontanari, International Journal of Mechanical Sciences 122 (2017), 63–78.
[17] Curve Fitting Toolbox: for Use with MATLAB®: User's Guide. Natick, MA: MathWorks, 2018.